Supplementary material

Atomically mixed catalysts on a 3D thin-shell TiO_2 for dual-modal chemical detection and neutralization

Joonchul Shin,‡[a] Geonhee Lee,‡[b] Myungwoo Choi,‡[d] Huiwon Jang,[c] Yunsung Lim,[c] Gwang-Su Kim,[a] Sang-Hyeon Nam,[c] Seung-Hyub Baek,[a] Hyun-Cheol Song,[a,e,f] Jihan Kim,[c] Chong-Yun Kang,[a] Jeong-O Lee,[b] Seokwoo Jeon,*[d] Donghwi Cho,*[b] and Ji-Soo Jang*[a]*

[a]Electronic Materials Research Center, Korea Institute of Science and Technology (KIST), Seoul 02792, Republic of Korea

[b] Thin Film Materials Research Center, Korea Research Institute of Chemical Technology (KRICT), Daejeon 34114, Republic of Korea

[c] Department of Chemical and Biomolecular Engineering, Korea Advanced Institute of Science and Technology (KAIST), Daejeon 34141, Republic of Korea

[d] Department of Materials Science and Engineering, Korea University, Seoul 02841, Republic of Korea

[e] School of Advanced Materials Science and Engineering, Sungkyunkwan University (SKKU), Suwon 16419, Republic of Korea

[f] KIST-SKKU Carbon-Neutral Research Center, Sungkyunkwan University (SKKU), Suwon 16419, Republic of Korea

‡ These authors contributed equally to this work: J. Shin, G. Lee, and M. Choi

* Correspondence should be addressed to J.-O. Lee (email: jolee@krict.re.kr), S. J. (jeon39@korea.ac.kr), D. Cho (roy.cho@krict.re.kr), J.-S. Jang (wkdwltn92@kist.re.kr)

Keywords: 3D TiO_2, polyelemental metal nanoparticles, photoactivation, chemical detection, photocatalytic degradation

Materials.

Chloroplatinic acid hexahydrate ($H_2PtCl_6 \cdot 6H_2O$), Potassium tetrachloropalladate(II) (K_2PdCl_4), Nickel(II) nitrate hexahydrate ($Ni(NO_3)_2 \cdot 6H_2O$), and Cobalt(II) chloride hexahydrate ($CoCl_2 \cdot 6H_2O$) were purchased from Sigma-Aldrich (St. Louis, USA).

Preparation of the periodic 3D nanostructured epoxy template

An epoxy-based photoresist (PR) (SU-8, Microchem) with a thickness of ~ 10 μm was spin-coated at 3000 rpm for 30 sec on a SiO_2/Si substrate which was treated by air plasma (CUTEMP, Femtoscience) for 2 min under the conditions (flow rate of 45 sccm, pressure of 40 mTorr, and power of 60 W). The PR layer was soft baked at 65 ℃ for 30 min and 95 ℃ for 30 min in 2 steps. Then, the PR-coated substrate was softly contacted with a conformal poly-dimethyl-siloxane (PDMS) phase mask that consisted of a square array of holes with a diameter of ~ 480 nm, a depth of ~ 420 nm, and a periodicity of ~ 600 nm. After the process of proximity-field nanopatterning (PnP) technique including conventional lithographic procedures (a post-baking step with a 65 ℃ hot plate for 7 min, a developing step (SU-8 developer, Microchem), a rinsing step with deionized water, and a drying process), a periodic 3D nanostructured epoxy template was prepared.

Preparation of 3D TiO_2

A thin TiO_2 layer (30, 50, and 70 nm) was conformally deposited on the pre-fabricated 3D nanostructured epoxy template by atomic layer deposition (ALD) technique at 90 ℃ (Nexusbe Co., Ltd) [1–3]. Tetrakis-dimethyl-amido titanium (TDMAT) (UP Chemical) and distilled water were selected as the precursor and reactant, respectively. Each ALD cycle consisted of a sequential process of precursor dose (TDMAT 100 sccm for 1 sec), purging (Ar 100 sccm for 30 sec), reactant dose (distilled water 100 sccm for 1 sec), and pursing (Ar 100 sccm for 25

sec). The deposition rate was approximately 0.75 Å per cycle. Then, the epoxy component of the TiO_2-coated polymeric template was selectively removed through thermal treatment in 2 steps: 350 ℃ for 5 hours at a heating rate of 2 ℃ min^{-1} and 500 ℃ for 2 hours at a heating rate of 1 ℃ min^{-1}.

Characterization

The structural feature of the 3D TiO_2 samples was characterized using field-emission scanning electron microscopy (FESEM, Magellan 400, FEI Co.) operated at an accelerating voltage of 5-10 kV. The TEM analysis for inspecting the sharply cut cross-section of 3D TiO_2 was done by carefully cracking the sample to avoid structural collapse. The absorbance measurements were performed by using UV-VIS spectrophotometry (UV-2550, Shimadzu). The mass of 3D TiO_2 was measured by using a Sartorius LE225D analytical balance. The scanning electron microscopy (SEM, S-4800, Hitachi) was performed to observe a cross-sectional view of the 3D TiO2. The PE NPs were analyzed by the transmission electron microscopy with energy dispersive spectrometry (EDS) mapping analysis (TEM, FIELD EMISSION GUN Tecnai G2 F20 X-TWIN). X-ray Diffraction (XRD) pattern for PE NPs was carried out using a Rigaku D/MAX 2500PC at 4˚/min scan rate with 1.5418 Å radiation. An Electronic Paramagnetic Resonance (EPR) spectrometer was performed to quantify difference of oxygen vacancy defect between a pristine TiO_2 powder and an IPL-treated TiO_2 powder at 9217.7 MHz, 0.998 mW power, 30 sec scan, and 400 G amplitude (JES-FA100, JEOL). The elemental composition of the chemicals in PE NPs was explored by X-ray photoelectron spectroscopy (XPS, VersaProbe, Ulvac-PHI) with monochromated Al Kα radiation (1486.6 eV).

Gas sensing measurement

Gold electrodes (100 nm thickness, 150 μm interspacing distance between two electrodes) were deposited on the surface of 3D TiO_2, Pt@TiO_2, PtPd@TiO_2, PtPdNi@TiO_2, PtPdCo@TiO_2, and PtPdNiCo@TiO_2 by using a thermal evaporation system in order to evaluate the gas-sensing performance. The gas sensing properties were conducted on a gas testing Micro probe system (MPS-CHH8C, NEXTRON, KOREA). Each electrode was directly contacted on the Rh wire probe in the gas testing Micro probe system. Before the measurement, the electrical properties of the gas sensor were saturated under 365 nm UV illumination (VL-4LC, VILBER, FRANCE) in air gas for several hours. Subsequently, the target gases were injected into the gas chamber system by controlling the gas flow through using an automated mass flow controller (AFC 600, ATOVAC, KOREA): three repeating cycles of dry air for 20 min, and the target gases (NO_2, NH_3, C_7H_8, H_2S, C_6H_6, and C_3H_6O balanced with air) for 10 min (1 cycle: 30 min) at a total flow of 1000 sccm. The resistance signals from the gas response were measured by a multi-channel switching matrix (Keithly 3700A) at a 5 V DC bias using a source meter (Keithley 2400).

In order to evaluate the sensor performances, the sensitivity value (%) was calculated as follows.

$$Sensitivity\ (\%) = \left|\frac{R_0 - R_a}{R_0}\right| \times 100$$

R_o is the initial resistance and Ra is the resistance value changed after sensing materials reacted with target gas under UV illumination. The sensor performance was evaluated by averaging the sensor sensitivity of three repeated measurements.

Photocatalytic performance test

Before the pollutant degradation experiments, TiO_2, PtPd@TiO_2, and PtPdNiCo@TiO_2 on SiO_2 substrate were fabricated with a size of 1 x 1 cm (1 cm^2) and then the sample was placed

in a plastic dish. After adding 3mL of the MB solution in deionized water (10^{-5} M) to the plastic dish with the sample, the portable UV light source (VL-4LC, VILBER, FRANCE) was placed on top of the plastic dish and UV light (wavelength of 365 nm) was irradiated with a intensity of 1.2 mW/cm^2. Each MB solution (2 mL) was taken after the exposing times of 1, 3, and 5 hours and investigated by measuring the absorbance in the range from 250 to 700 nm with a UV-Visible spectroscopy (UV-2550, SHIMADZU, JAPAN).

The Photocatalytic performance of PE NPs@3D TiO_2 was evaluated by calculating the decomposition ratio of methylene blue (MB) under UV illumination (MB initial concentration: 10^{-5} mM). The 3D TiO_2 samples were placed into the 6 well plastic dish and each MB solution of 3 ml was added. The UV exposure time to the samples in MB solution was controlled up to 5 hours. After the exposure, the MB solutions were collected and their optical properties in the range of 200 – 600 nm were measured by using a UV-vis spectroscopy (UV-2550, Shimadzu, Kyoto, Japan). The absorbance peaks at 550 nm were measured for evaluating the photocatalytic efficiency based on the following equation where C_o is the initial concentration of MB solution and C_t is the decomposed MB concentration from UV illumination.

$$Photocatalytic\ efficiency = \frac{C_t}{C_0}$$

Collectively, the MB photocatalytic performance of the samples was evaluated by averaging the photocatalytic efficiency of 3 repeated experiments.

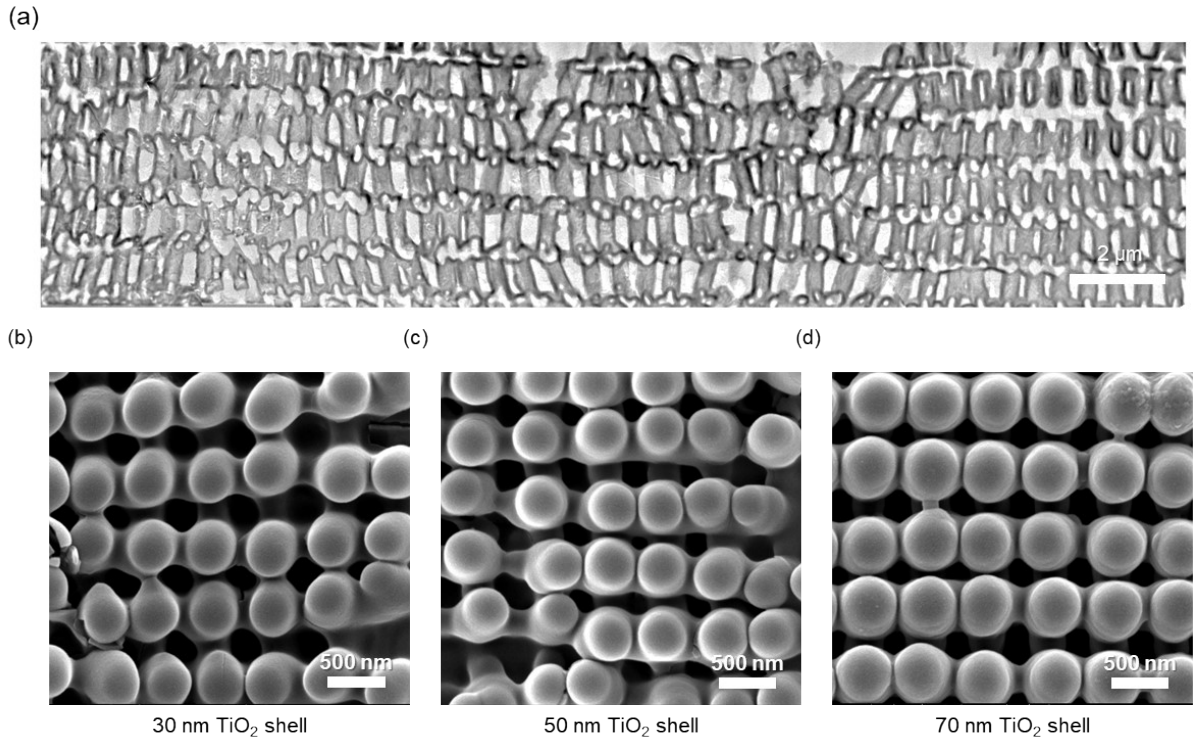

Fig. S1. Cross-sectional view SEM images (a) and top-view SEM images of 3D TiO_2 shell and wall-thickness with (b) 30 nm, (c) 50 nm, and (d) 70 nm by controlling ALD deposition cycles.

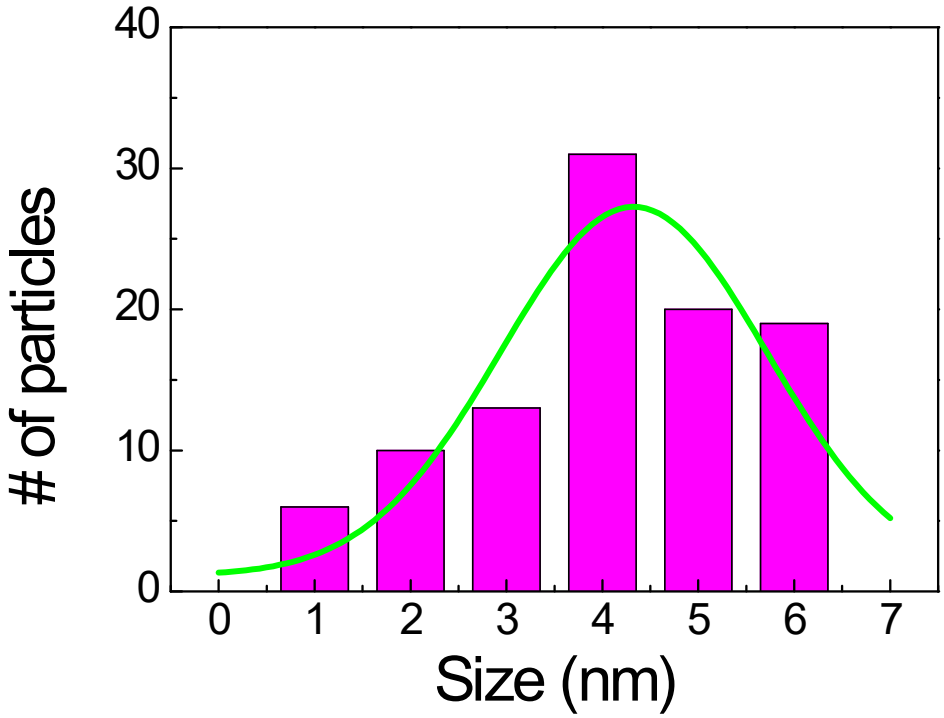

Fig. S2. Size distribution of PtPdNi nanoparticles with 4.03 ± 1.01 nm as averaged from the total particles.

(a)

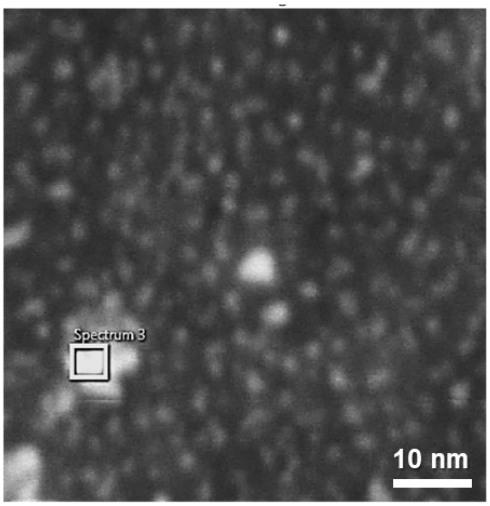

(b)

Element	Wt%	Atomic%
Pt	1.49	0.19
Pd	9.47	2.25
Ni	2.89	1.24
Co	10.34	4.43
Ti	25.91	13.66
O	49.29	77.79
Cl	0.61	0.43

Fig. S3. Point EDS analysis for qualifying coexistence of quaternary alloys (PtPdNiCo) on 3D thin-shell TiO_2. (a) STEM image for the quaternary nanoparticles. (b) Weight and atomic percentage of each atom from the alloys on the 3D TiO_2 shell.

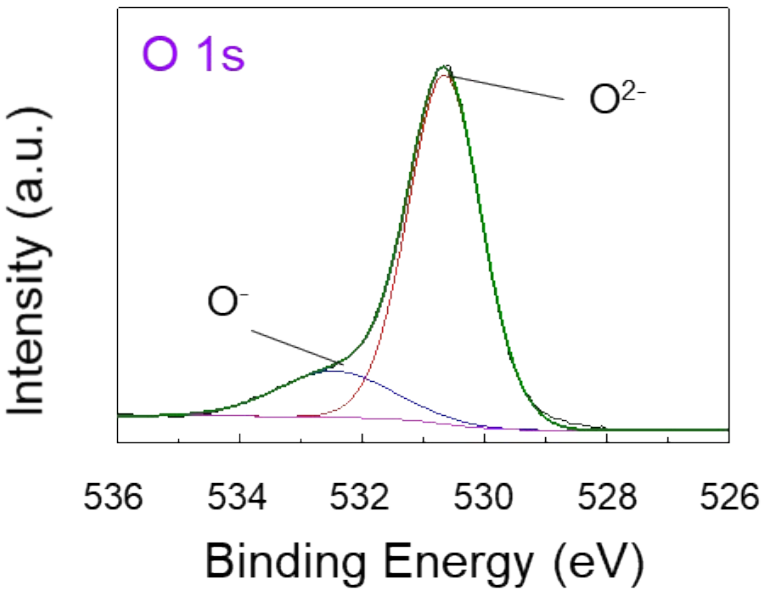

Fig. S4. O 1s peak of the bare TiO_2 in the XPS spectrum.

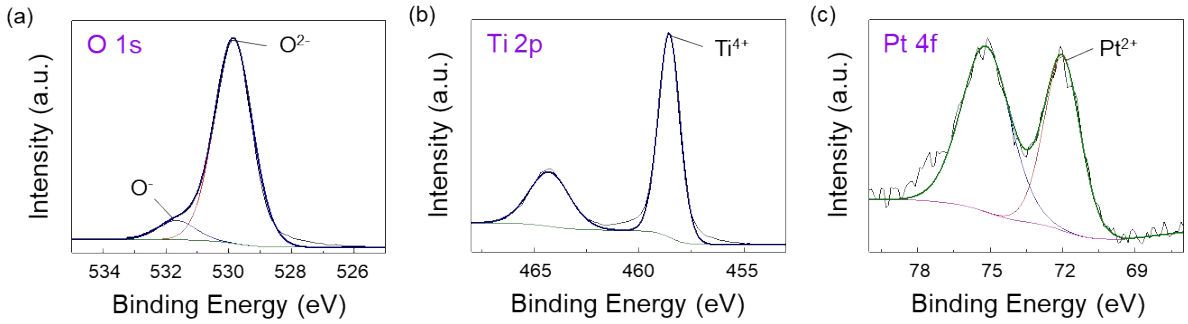

Fig S5. XPS spectrum of urinary (Pt) nanoparticles on 3D TiO_2 shell. (a) O 1s peak, (b) Ti 2p peak, and (c) Pt 4f peak

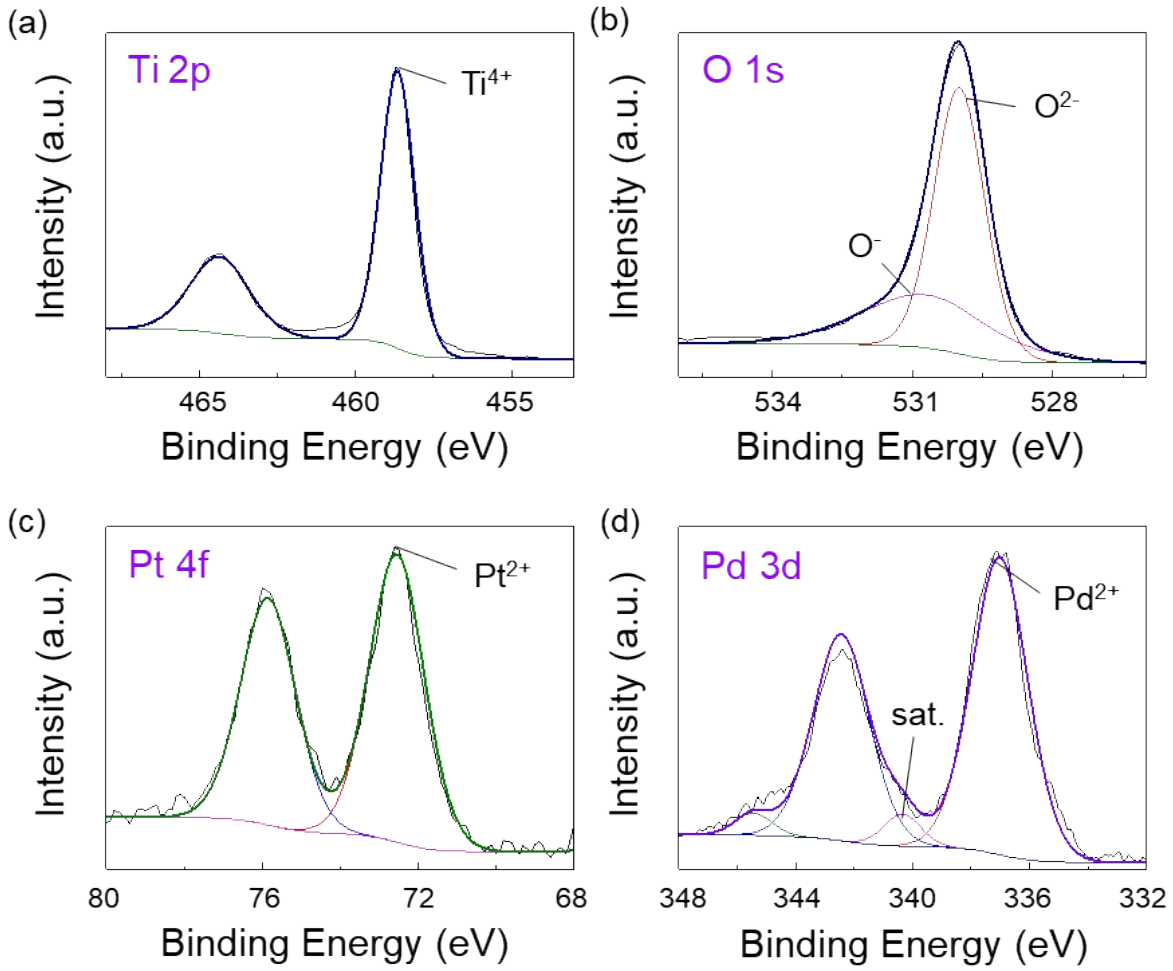

Fig. S6. XPS spectrum of binary (PtPd) nanoparticles on 3D TiO_2 shell. (a) Ti 2p peak, (b) O 1s peak, (c) Pt 4f peak, and (d) Pd 3d peak.

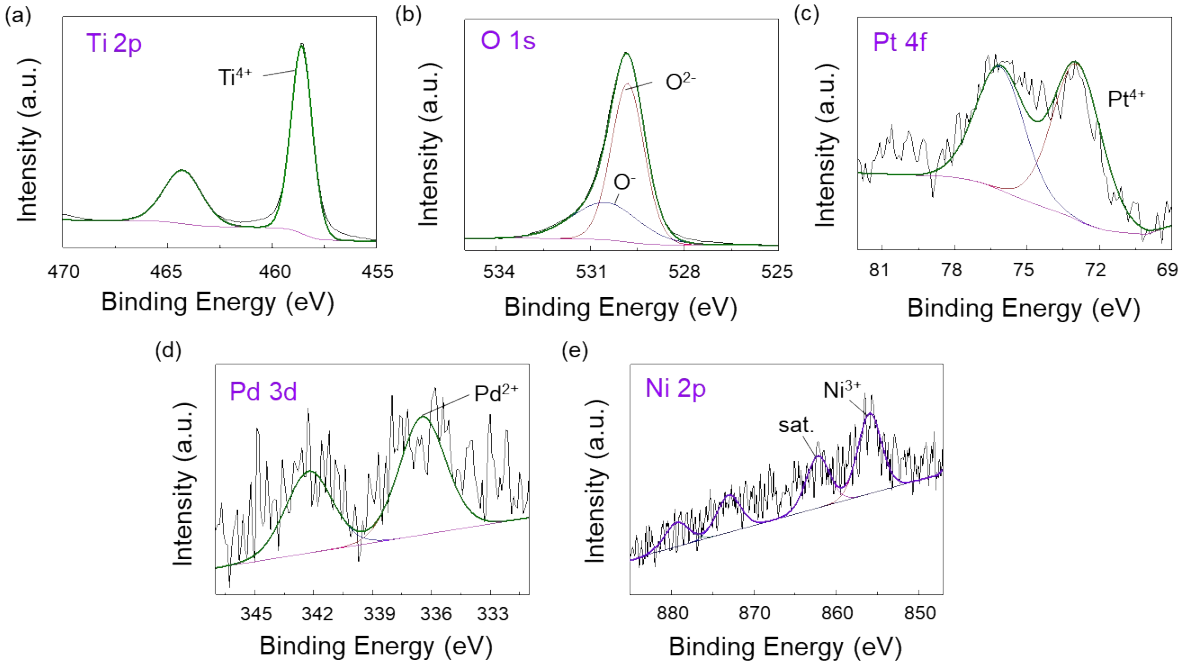

Fig. S7. XPS spectrum of ternary (PtPdNi) nanoparticles on 3D TiO_2 shell. (a) Ti 2p peak, (b) O 1s peak, (c) Pt 4f peak, (d) Pd 3d peak, and (e) Ni 2p peak.

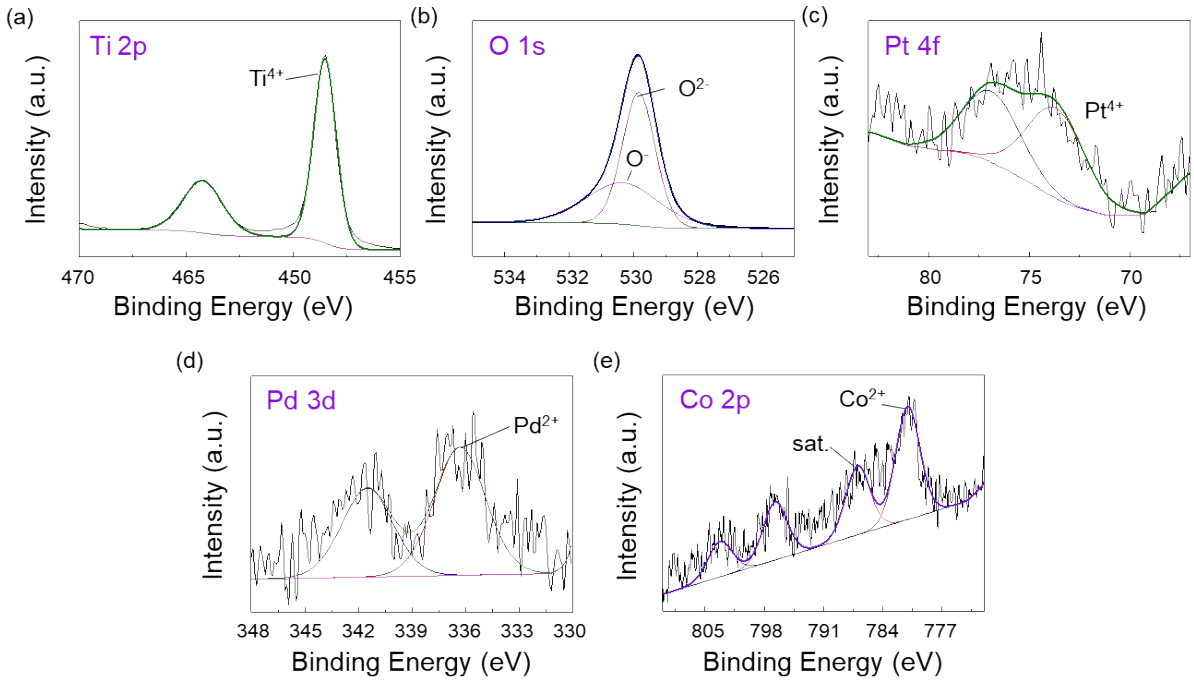

Fig. S8. XPS spectrum of ternary (PtPdCo) nanoparticles on 3D TiO_2 shell. (a) Ti 2P peak, (b) O 1s peak, (c) Pt 4f peak, (d) Pd 3d peak, and (e) Co 2p peak.

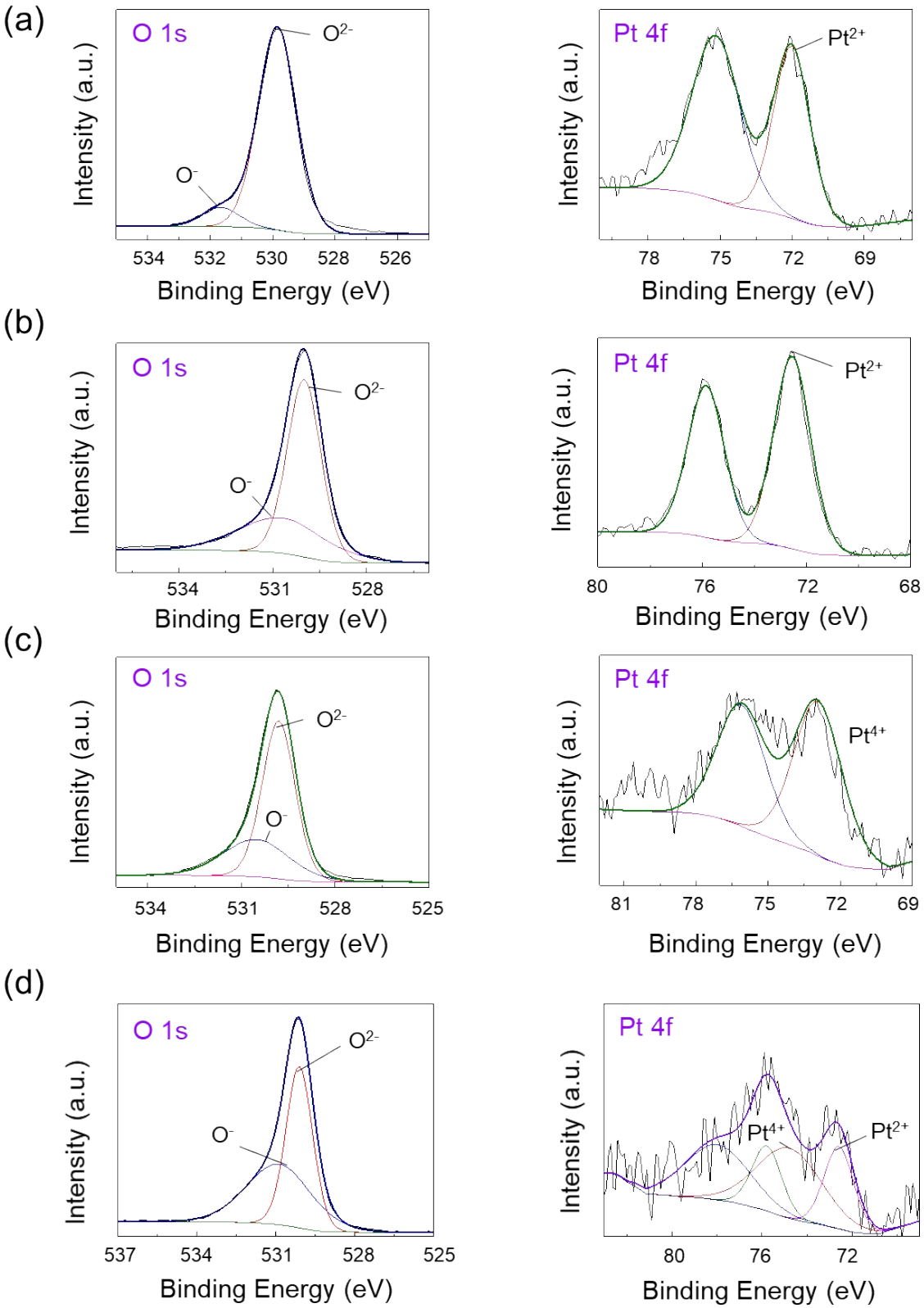

Fig. S9. Comparison of the ratio of O^-/O^{2-} and existence of Pt^{2+} and Pt^{4+} in polyelemental nanoparticles as raising the number of elements. (a) unary, (b) binary, (c) ternary and (d) quaternary phase in the XPS spectrum.

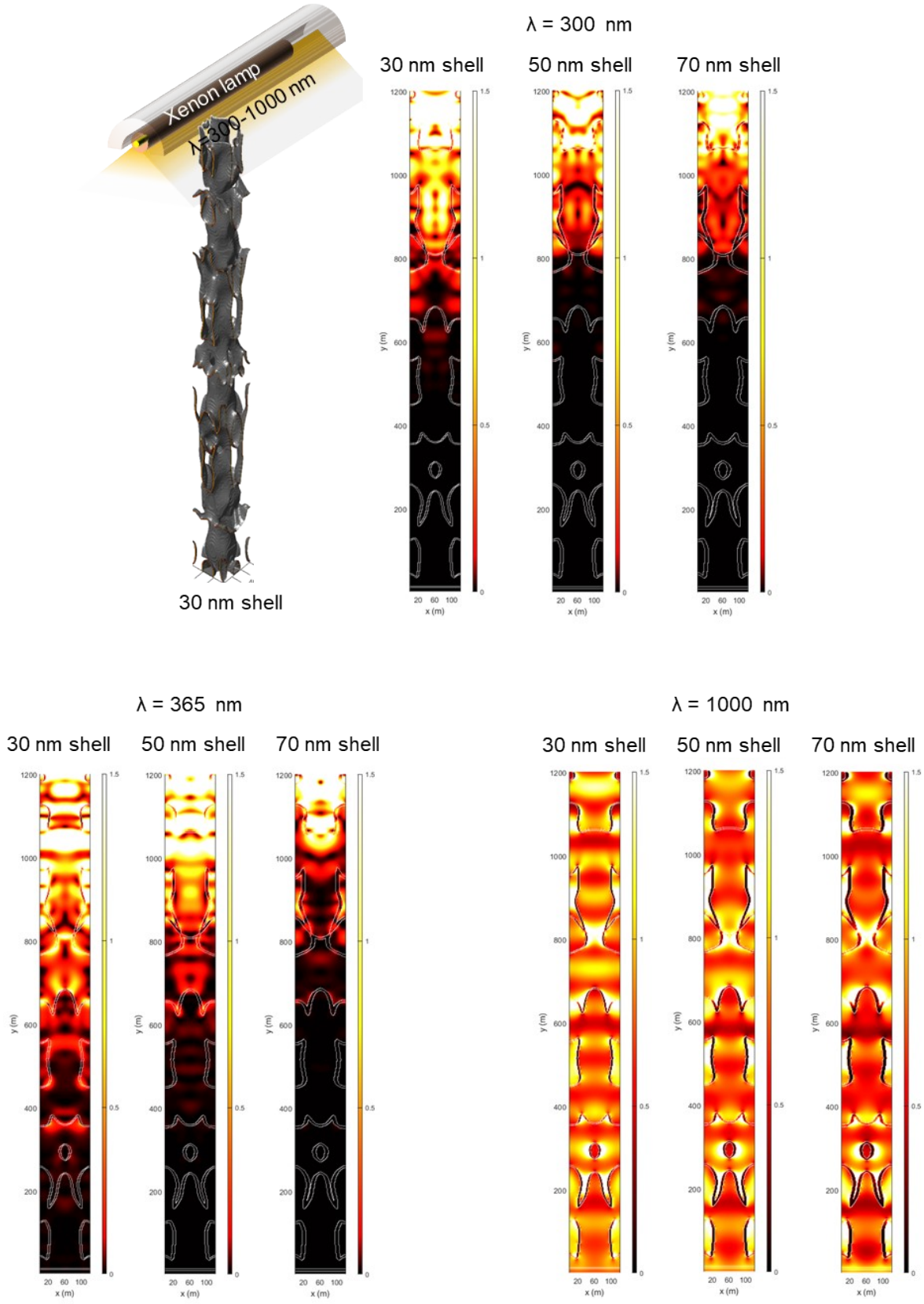

Fig. S10. Simulation for finite element modeling on 3D TiO_2 structure. Comparison of E-field intensity distribution when penetrating light source to 3D TiO_2 shell (30, 50, and 70 nm) with multi-wavelength (300, 365, and 1000 nm).

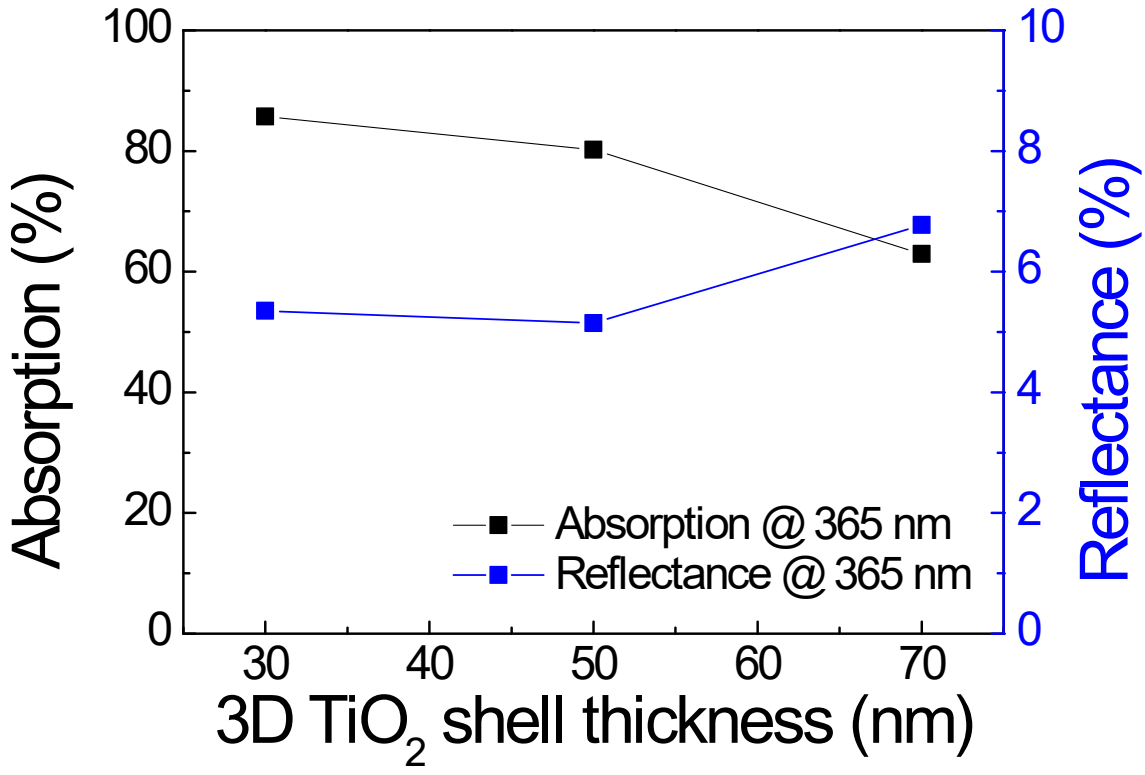

Fig. S11. Shell thickness effect of 3D TiO_2 towards light absorption and reflectance at the wavelength of 365 nm.

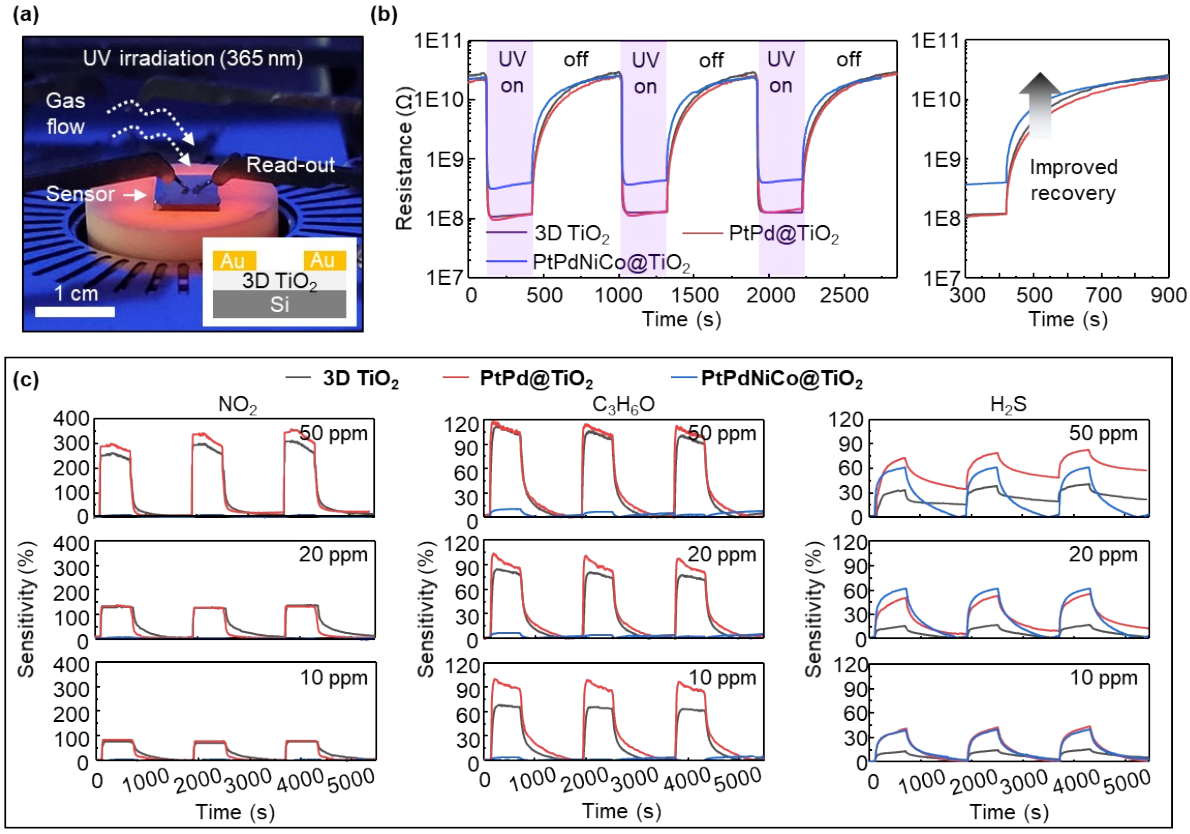

Fig. S12. Photoactivated, chemoresistive gas sensing results of PE NPs@3D TiO_2. (a) Digital image of experimental setup with UV irradiation system. (b) Response transients of 3D TiO_2 (black), PtPd@TiO_2 (red) and PtPdNiCo@TiO_2 (blue) to UV illumination on/off at 5 V. (c) Calculated responses of 3D TiO_2, PtPd@TiO_2, and PtPdNiCo@TiO_2 to different gases: NO_2 (left), C_3H_6O (center) and H_2S (right) as a function of controlled concentrations of 10, 20 and 50 ppm under UV illumination at 5 V.

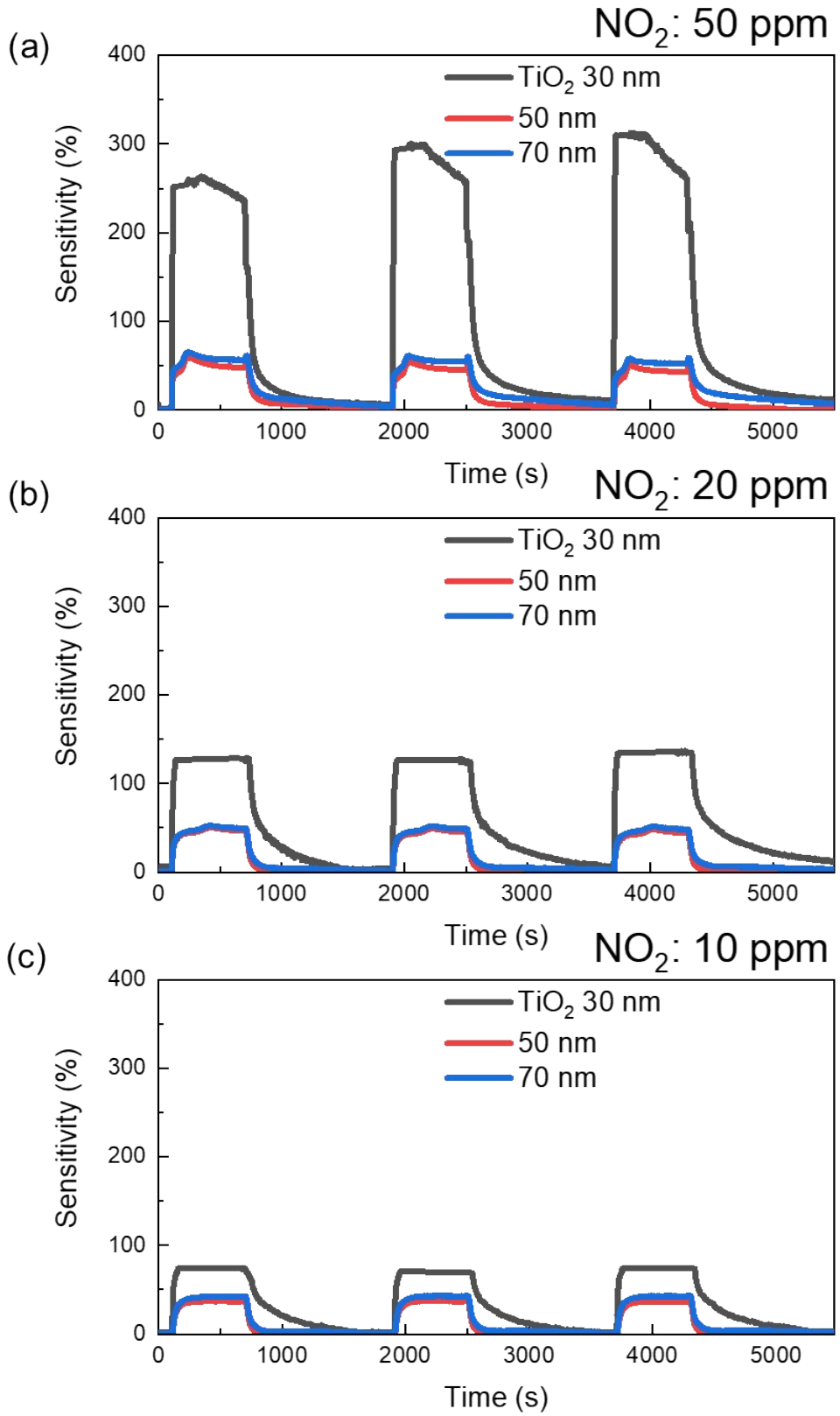

Fig. S13. TiO_2 thickness-dependent chemoresistive response towards NO_2 gas molecules. Chemoresistive response to NO_2 gas molecules (a) 50 ppm (b) 20 ppm (c) 10 ppm as a function of 3D TiO_2 shell thickness

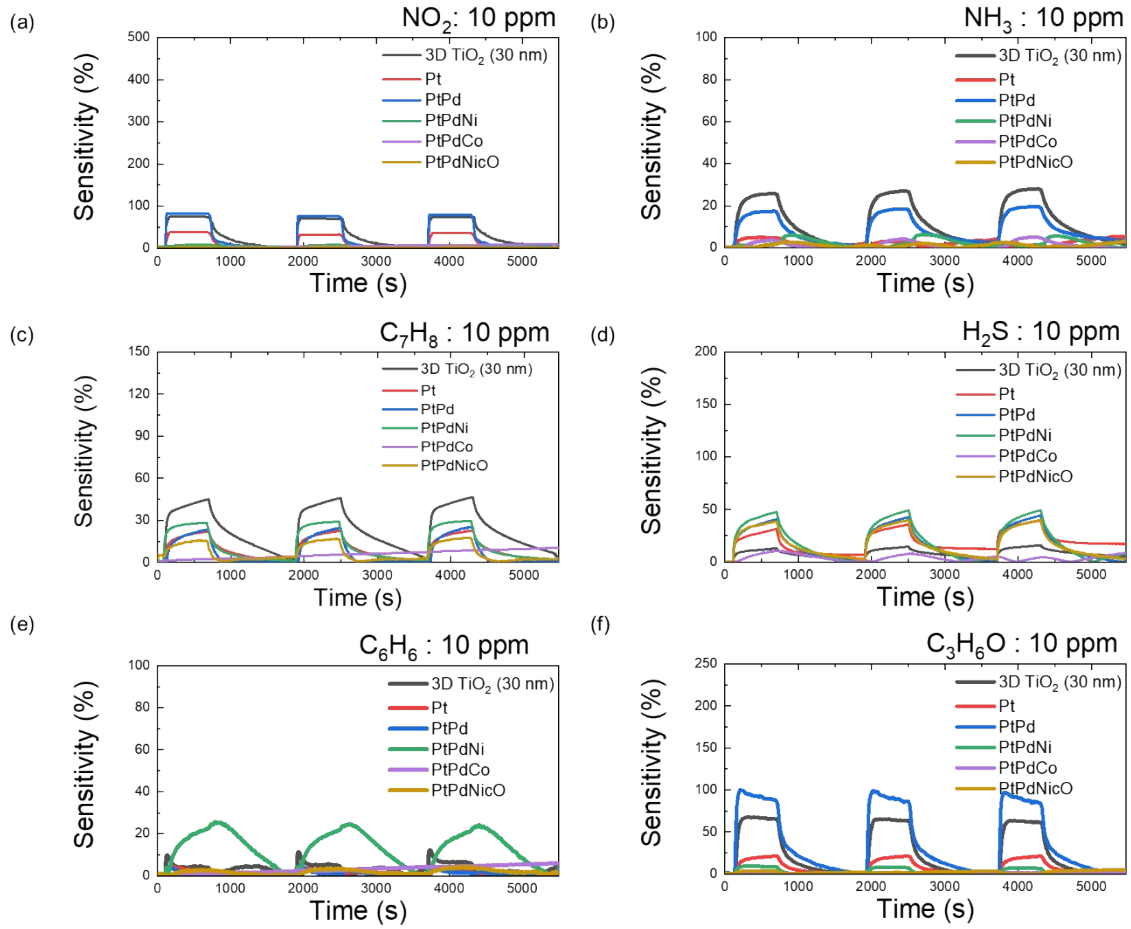

Fig. S14. Gas response curves using six different gases. Gas sensing test with 3D TiO_2, Pt@TiO_2, PtPd@TiO_2, PtPdNi@TiO_2, PtPdCo@TiO_2, and PtPdNiCo@TiO_2 toward 10 ppm of (a) NO_2, (b) NH_3, (c) C_7H_8, (d) H_2S, (e) C_6H_6 and (f) C_3H_6O.

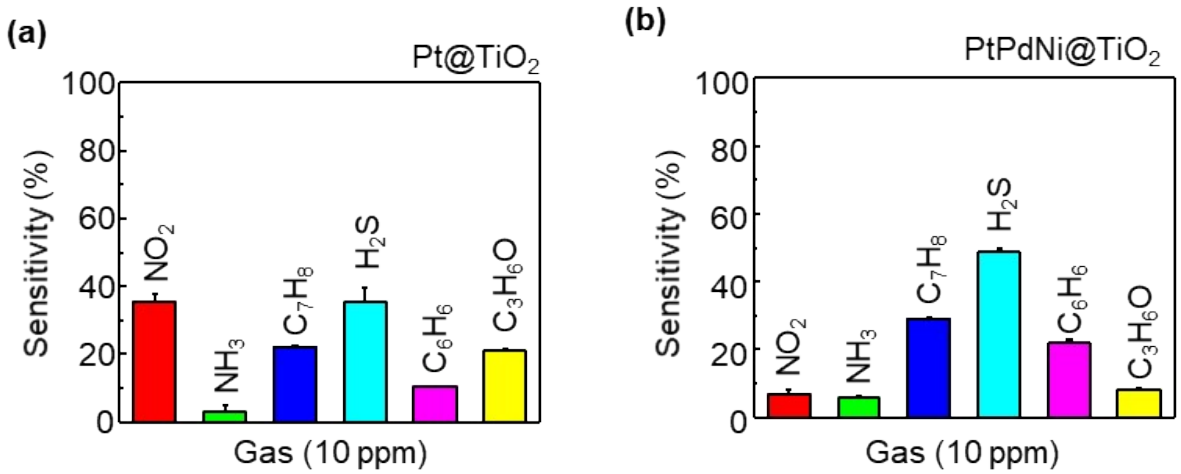

Fig. S15. Gas sensing properties of (a) $Pt@TiO_2$ and (b) $PtPdNi@TiO_2$ for tracking gas selectivity change.

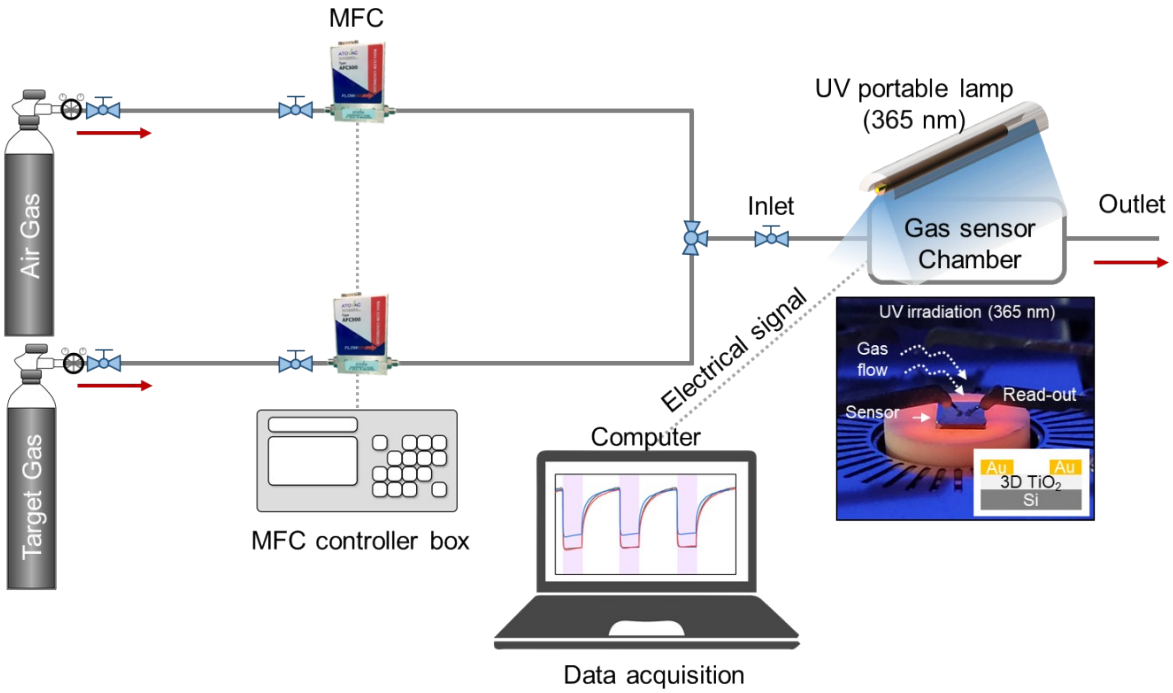

Fig. S16. Schematic diagram of the gas sensor measurement system for detection against toxic gases under UV irradiation (365 nm wavelength).

A gas sensing system (Micro Probe system, MPS-CHH8C, NEXTRON, KOREA) with a controller system of UV exposure was prepared. The gas sensing tests were carried out in the gas chamber system under ambient conditions. Air gas was used as a carrier gas to dilute the concentration of analytes (NO_2, NH_3, C_7H_8, H_2S, C_6H_6, and C_3H_6O) and purged the gas sensing chamber for sensing cycle repetition using a mass flow controller (AFC 600, ATOVAC, Korea) for a flow rate of 1000 sccm constantly. The UV illumination system (Vilber Lourmat, 6W, 365 wavelength) was placed on the top of the gas chamber system (λ=365 nm and power reaching on the sensor ~ 1.17 mW). The sensor device was placed into a sample holder and stabilized with applied 5 V using Keithley 2612B instrument) in an Air-gas for several hours under UV illumination. After stabilization, the gas sensor test was performed by switching the diluted target gas to 10, 20, and 50 ppm for 10 min, and air gas for 20 min in three times repeat. Reading of the measured sensor data and controlling of gas flow were systematically conducted by using KI2600S-3706A-GMC1200 Multi-channel measurement software (I.V solution, KOREA). In addition, the three cycles of UV turn-on for 5 min and off for 10 min were studied for the UV response tests.

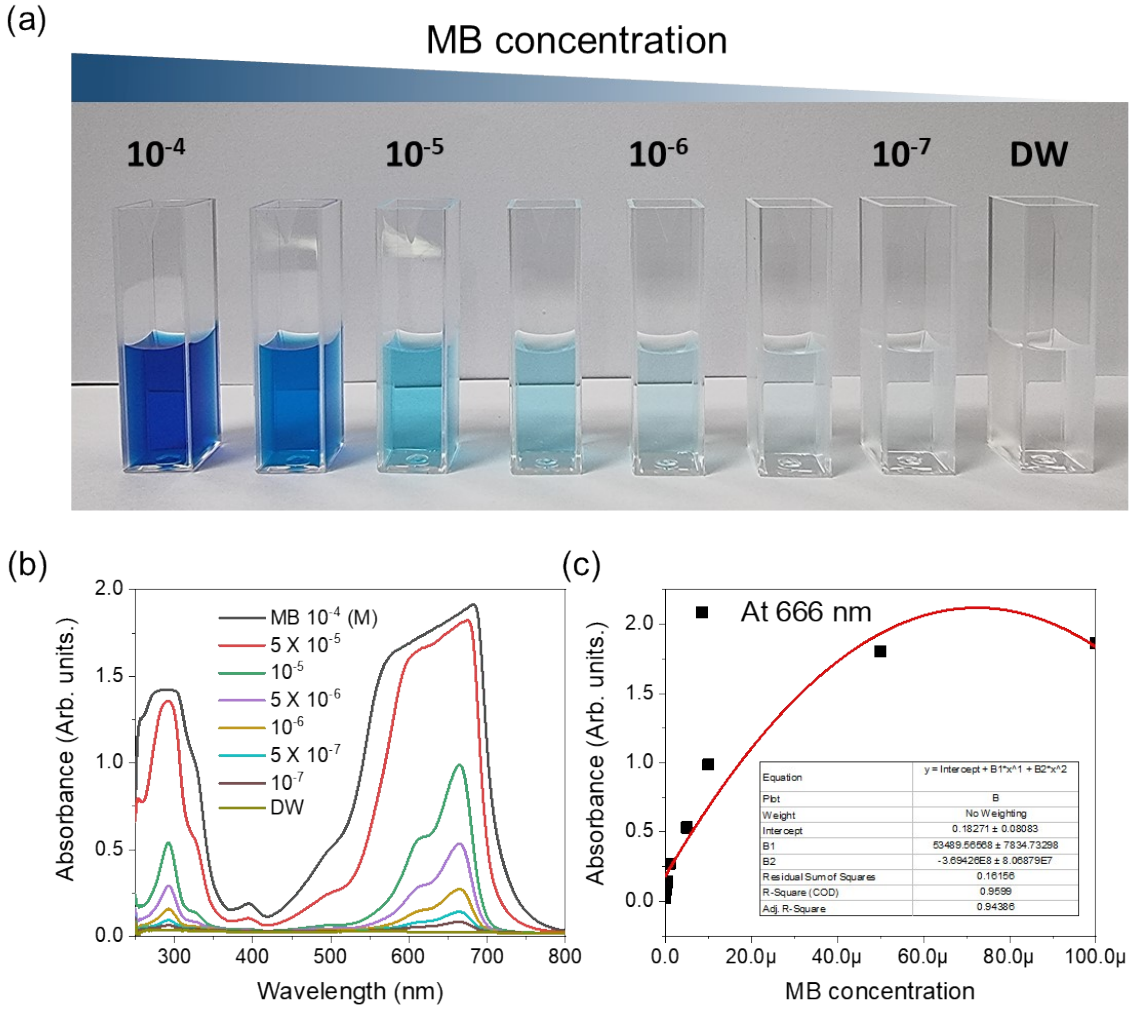

Fig. S17. Calibration data of Methylene blue concentration in UV analysis. (a) a photograph of MB solutions as a function of the concentration. (b) UV-vis spectra from (a). (c) a curve fitting data for calibration of MB concentration.

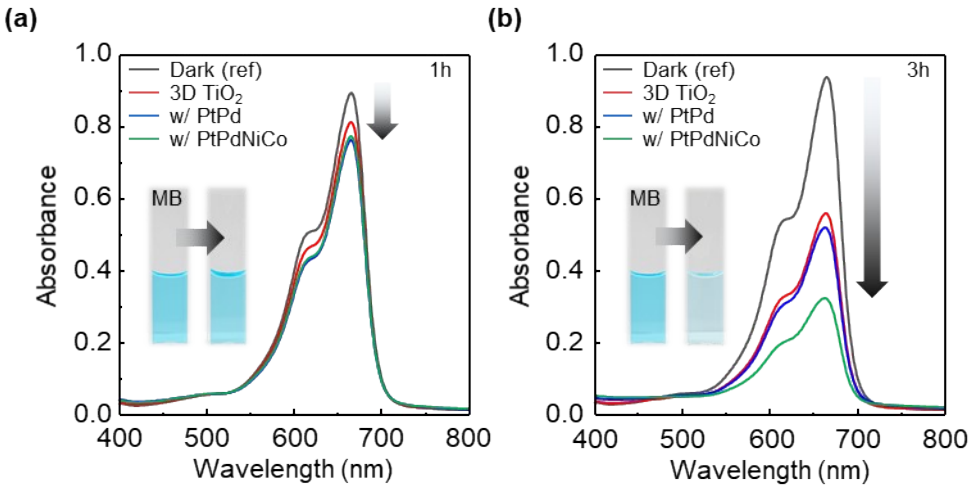

Fig. S18. Time-dependent absorbance change of methylene blue (MB) solutions with no sample under darkness (black), 3D TiO_2 (red), PtPd@TiO_2 (blue), PtPdNicO@TiO_2 (green) under UV exposure for a) 1 hour and b) 3 hours.

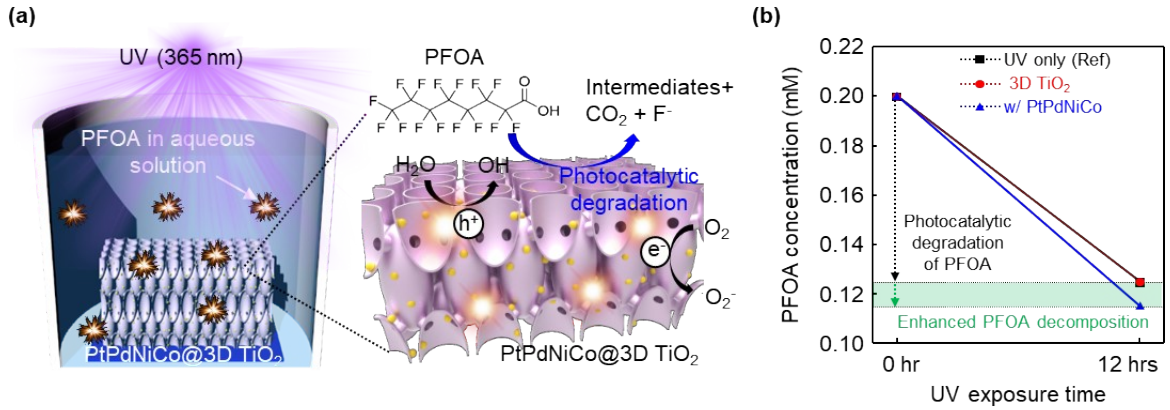

Fig. S19. (a) Schematic illustration of the PFOA photodegradation application using PtPdNiCo@TiO_2 under UV illumination. b) Measured PFOA concentration changes after 12 hours of photocatalytic degradation of PFOA.

Catalyst type		Light source (Power)	Irradiation time	Sample size	Weight	C/C_0	Reference
Powder type	Sb-doped TiO_2	Xe light (0.8 W/cm^2)	~ 1 hour	-	0.05 g	98.2%	[4]
	Degussa P25 Commercial TiO_2 nanoparticles	UV light (1 mW/cm^2)	5 hours	-	-	82%	[5]
	Cu, Zn tetracarboxy-phthalocyanines sensitized TiO_2	Visible light (90 mW)	2 hours	-	TiO_2 Powder (0.1-0.6 g)	~ 40%	[6]
	TiO_2 pretreated with NaOH	Xe light (300 W)	2 hours	-	20 mg	~ 82%	[7]
Nanotube type	TiO_2-coated Anodisc membrane	UV light (1.5 mW/cm^2)	~ 4 hours	0.2 cm × 0.2 cm	-	~ 38%	[8]
	Anodized TiO_2 nanotube	Xe light (150 W)	5 hours	1.0 cm × 1.0 cm	-	~ 80%	[9]
	Curcumin modified TiO_2 nanotube	Visible light (18 W)	3 hours	1.5 cm × 2.5 cm	-	~ 23%	[10]
Film type	TiO_2 thin film	UV light (1 mW/cm^2)	5 hours	2.0 cm × 2.5 cm	-	24%	[4]
	g-C3N4/TiO_2 films	Visible light (64 mW/cm^2)	3 hours	2.0 cm × 5.0 cm	-	~ 65%	[11]
	3D Ag/TiO_2 nanocomposite	Xe light (153 mW)	2.5 hours	3.0 cm × 3.0 cm	-	79.8%	[12]
	Undoped TiO_2 film	UV light (1.5 mW/cm^2)	3 hours	1.0 cm × 2.0 cm	-	~ 28%	[3]
	N-doped TiO_2 film	UV light (1.5 mW/cm^2)	3 hours	1.0 cm × 2.0 cm	-	~ 29%	[3]
	3D Undoped TiO_2 film	UV light (1.5 mW/cm^2)	3 hours	1.0 cm × 2.0 cm	-	~ 65%	[3]
	3D N-doped TiO_2 film	UV light (1.5 mW/cm^2)	3 hours	1.0 cm × 2.0 cm	-	~ 61%	[3]
	Graphene quantum dot (GQD) decorated 3D TiO_2 film	UV light (1.5 mW/cm^2)	4 hours	2.5 cm × 2.5 cm	-	60%	[13]
	Graphene quantum dot (GQD) decorated 3D TiO_2 film	Visible light (5.5 mW/cm^2)	4 hours	2.5 cm × 2.5 cm	-	55%	[13]
	PtPdNiCo@3D TiO_2	UV light (1.2 mW/cm^2)	5 hours	1.0 cm × 1.0 cm	0.18 mg	72%	**This work**

Table S1. MB degradation performances in other literatures

Reference

1 D. Cho, J. M. Suh, S. Nam, S. Y. Park, M. Park, T. H. Lee, K. S. Choi, J. Lee, C. Ahn, H. W. Jang, Y. Shim and S. Jeon, *Adv. Sci.*, 2021, **8**, 2001883.

2 J. M. Suh, D. Cho, S. Lee, T. H. Lee, J. Jung, J. Lee, S. H. Cho, T. H. Eom, J. Hong, Y. Shim, S. Jeon and H. W. Jang, *Small Methods*, 2021, **5**, 2100941.

3 S. Cho, C. Ahn, J. Park and S. Jeon, *Nanoscale*, 2018, **10**, 9747–9751.

4 J. Moon, H. Takagi, Y. Fujishiro and M. Awano, *J. Mater. Sci.* 2001, **36**, 949-955.

5 C. Ahn, J. Park, D. Kim and S. Jeon, *Nanoscale*, 2013, **5**, 10384.

6 W. Vallejo, C. Diaz-Uribe and Á. Cantillo, *Journal of Photochemistry and Photobiology A: Chemistry*, 2015, **299**, 80–86.

7 C. Hou, B. Hu and J. Zhu, *Catalysts*, 2018, **8**, 575.

8 M. Kemell, V. Pore, J. Tupala, M. Ritala and M. Leskelä, *Chem. Mater.*, 2007, **19**, 1816–1820.

9 D. Wang, Y. Liu, B. Yu, F. Zhou and W. Liu, *Chem. Mater.*, 2009, **21**, 1198–1206.

10 Department of Physics, Faculty of Science, Silpakorn University, Sanam Chandra Palace Campus, Nakhon Pathom, Thailand 73000 and M. Aiempanakit, *Int. J. Electrochem. Sci.*, 2019, 1954–1967.

11 N. Boonprakob, N. Wetchakun, S. Phanichphant, D. Waxler, P. Sherrell, A. Nattestad, J. Chen and B. Inceesungvorn, *Journal of Colloid and Interface Science*, 2014, **417**, 402–409.

12 Z.-J. Zhao, S. H. Hwang, S. Jeon, B. Hwang, J.-Y. Jung, J. Lee, S.-H. Park and J.-H. Jeong, *Sci Rep*, 2017, **7**, 8915.

13 H. Yoon, K. Lee, H. Kim, M. Park, T. G. Novak, G. Hyun, M. S. Jeong and S. Jeon, *Adv. Sustainable Syst.*, 2019, **3**, 1900084.